communications earth & environment

ARTICLE

https://doi.org/10.1038/s43247-022-00457-y OPEN

Synchronous vegetation response to the last glacial-interglacial transition in northwest Europe

Stefan Engels[1,2✉], Christine S. Lane[3], Aritina Haliuc[4,5], Wim Z. Hoek[6], Francesco Muschitiello[3], Ilaria Baneschi[7], Annerieke Bouwman[8], Christopher Bronk Ramsey[9], James Collins[10], Renee de Bruijn[11], Oliver Heiri[12], Katalin Hubay[13], Gwydion Jones[14], Andreas Laug[15], Josef Merkt[16], Meike Müller[17], Tom Peters[1], Francien Peterse[8], Richard A. Staff[18], Anneke T. M. ter Schure[1,19], Falko Turner[20], Valerie van den Bos[1,21] & Frederike Wagner-Cremer[6]

The North Atlantic region experienced abrupt high-amplitude cooling at the onset of the Younger Dryas stadial. However, due to chronological uncertainties in the available terrestrial records it is unclear whether terrestrial ecosystem response to this event was instantaneous and spatially synchronous, or whether regional or time-transgressive lags existed. Here we use new palynological results from a robustly dated lake sediment sequence retrieved from lake Hämelsee (north Germany) to show that vegetation change started at 12,820 cal. yr BP, concurrent with the onset of changes in local climate. A comparison of the Hämelsee results to a compilation of precisely dated palynological records shows instant and, within decadal-scale dating uncertainty, synchronous response of the terrestrial plant community to Late-Glacial climate change across northwest Europe. The results indicate that the environmental impact of climate cooling was more severe than previously thought and illustrates the sensitivity of natural terrestrial ecosystems to external forcing.

[1] Institute for Biodiversity and Ecosystem Dynamics, University of Amsterdam, Science Park 904, 1090 GE Amsterdam, The Netherlands. [2] Department of Geography, Birkbeck University of London, London WC1E 7HX, UK. [3] Department of Geography, University of Cambridge, Downing Place, Cambridge CB2 3EN, UK. [4] Section 4.3 Climate Dynamics and Landscape Evolution, GFZ German Research Centre for Geosciences, Potsdam D-14473, Germany. [5] Romanian Academy, Institute of Speleology, 5 Clinicilor, Cluj-Napoca 400006, Romania. [6] Department of Physical Geography, Faculty of Geosciences, Utrecht University, Postbus 80.115, 3508 TC Utrecht, The Netherlands. [7] Institute of Geosciences and Earth Resources IGG, National Research Council of Italy, Pisa, Italy. [8] Department of Earth Sciences, Faculty of Geosciences, Utrecht University, Postbus 80.115, 3508 TC Utrecht, The Netherlands. [9] Research Laboratory for Archaeology and the History of Art, University of Oxford, Dyson Perrins Building, South Parks Road, Oxford OX1 3QY, UK. [10] Section 5.1 Geomorphology, Organic Surface Geochemistry Laboratory, GFZ German Research Centre for Geosciences, Potsdam D-14473, Germany. [11] Geological Survey of the Netherlands, Postbus 80015, Utrecht 3508 TA, The Netherlands. [12] Geoecology, Department of Environmental Sciences, University of Basel, Klingelbergstrasse 27, CH-4056 Basel, Switzerland. [13] Institute for Nuclear Research, 4001 Debrecen P.O. Box 51 Hungary. [14] Department of Geography, College of Science, Swansea University, Singleton Park, Swansea SA2 8PP, UK. [15] Institute for Geosystems and Bioindication, Technische Universität Braunschweig, Braunschweig D-38106, Germany. [16] Ritter-Eccartstr 5, Herbertingen D-88518, Germany. [17] Institute of Geobotany, Leibniz Universität Hannover, Hannover D-30167, Germany. [18] Scottish Universities Environmental Research Centre (SUERC), University of Glasgow, Rankine Avenue, Scottish Enterprise Technology Park, East Kilbride G75 0QF, UK. [19] Centre for Ecological and Evolutionary Synthesis, Faculty of Mathematics and Natural Sciences, University of Oslo, Postboks 1066 Blindern, 0316 Oslo, Norway. [20] Institute of Tibetan Plateau Research, Chinese Academy of Sciences, 16 Lincui RoadChaoyang District Beijing 100101, People's Republic of China. [21] National Isotope Centre, GNS Science, Lower Hutt, 5010 Wellington, New Zealand. ✉email: s.engels@bbk.ac.uk

The North Atlantic region experienced abrupt and high-amplitude changes in climate during the Last Glacial/Interglacial Transition period (LGIT or Late-Glacial; ~15–11 ka BP[1]). The most prominent feature of North Atlantic LGIT records is the millennial-scale Younger Dryas (YD) stadial, characterised by abrupt cooling of summer temperatures by 2–8 °C in Europe[2]. A range of different drivers have been proposed to explain the transition to stadial conditions at the onset of the YD, including disruptions to ocean circulation patterns due to meltwater release from the Laurentide and Fennoscandian ice sheets, changes in greenhouse gas concentrations, solar forcing, high-scale volcanism, and the impact of an extra-terrestrial object[3–7]. Whilst uncertainties remain regarding global climate teleconnections during the LGIT, recent speleothem and ice core results indicate that the onset of cooling is synchronous (within decadal-scale dating uncertainty) across the North Atlantic region and beyond[6,8,9].

The large-amplitude cooling observed in northwest Europe at the onset of the YD is known to have impacted terrestrial vegetation[10–12] and the LGIT therefore provides a crucial period to develop our understanding of ecosystem response to external drivers such as climate change. However, our understanding of the timing of regional LGIT ecosystem response to climate change is hampered by chronological uncertainties in many of the available terrestrial sediment archives[13]. As an example, even the Lake Suigetsu record from Japan, which has a high-resolution radiocarbon dating strategy based on terrestrial plant macrofossils encased in varved sediments, shows 2-sigma dating uncertainties in the order of ±50 years[14]. Multi-decadal uncertainties preclude the assessment of regional leads and lags in ecosystem response as these can occur on a (sub-) decadal scale[15,16]. The use of a lower dating-resolution or tuning of lake sediment proxy signals to isotopic records from the Greenland ice cores, which allows transfer of the Greenland Ice Core Chronology (GICC05) time scale[17,18], further precludes a precise and independent comparison of available palaeoenvironmental data.

As a result of these dating uncertainties, conflicting theories exist as to when and how fast ecosystems responded to climate change at the onset of the YD. For instance, evidence from Europe[12] and Japan[14] suggests that vegetation and climate change occurred synchronously across large parts of the globe, within centennial-scale dating uncertainties. By contrast, other studies suggest centennial-scale off-sets between vegetation change in Europe and variations in the Greenland oxygen isotope records[19] or provide evidence for a time-transgressive palynological shift on a N-S gradient across northwest Europe at the onset of the YD[13].

Here we use high-resolution sedimentological, geochemical, and palaeoecological proxy records derived from a robustly dated lake sediment sequence retrieved from lake Hämelsee (north Germany; Fig. 1) to reconstruct vegetation and environmental dynamics across the LGIT (see Methods). The earliest changes in the pollen spectra associated with the onset of the YD can be observed at 12,820 ± 10 cal. yr BP concurrent with evidence of local climate cooling. In order to constrain the timing of terrestrial vegetation response to climate forcing across a wider region, we compare our results to three other northwest European sites that have high-resolution palynological datasets and robust chronological frameworks that closely constrain the biostratigraphical boundaries (Meerfelder Maar, Hässeldala Port and Kråkenes). We revised or re-modelled the existing age/depth models of these sites to enhance their accuracy and precision, and redefined the biostratigraphical transitions at the onset of the YD and the Holocene both visually and numerically. We specifically focus on the identification of early shifts in taxa that can act as 'canary species'[20,21], here defined as taxa that are most sensitive to external forcing such as climate cooling and that therefore show the most rapid responses. For instance, canary species are taxa that are at the edge of their spatial distribution or that are poorly-competitive. The combined results indicate regional synchroneity of terrestrial ecosystem responses to LGIT climate change throughout large parts of Europe, illustrating the sensitivity of natural terrestrial ecosystems to external forcing.

Results

The identification of five tephra-horizons[22] in the Hämelsee sediment record (Haem13), combined with varve-counting and AMS radiocarbon dating, provides an accurate and high-precision chronology for the Hämelsee record (Supplementary Table 1). The age/depth model for the Hämelsee sequence shows continuous sedimentation from 15,000 cal. yr BP onward, and has decadal-scale chronological precision in the late Allerød to early YD interval where a floating varve chronology is anchored to the absolute timescale using the Laacher See Tephra (LST) (Supplementary Fig. 1) which itself is dated to 13,006 ± 9yr[9]. The change from laminated to homogenous sediments, the decrease in loss-on-ignition values, as well as palaeoecological and geochemical proxy signals all show evidence for high-amplitude climatic change at lake Hämelsee (Fig. 2) synchronous with the onset of stadial conditions as observed in other European records[9]. For instance, the decreased contributions of glycerol dialkyl glycerol tetraether (GDGT)-0s produced by methanogenic archaea observed in the Hämelsee record from 12,825 (12,835–12,815, 2-sigma) cal. yr BP onward are potentially linked to higher levels of oxygen which can be the result of an increase in windiness facilitating lake mixing[23,24]. At the same time, we observe early changes in the chironomid fauna (e.g. increase in *Microtendipes pedellus*-type; Supplementary Fig. 2) and the chironomid-inferred July air temperature record shows an abrupt decline at 12,765 (12,775–12,755 cal. yr. BP (Fig. 2). The sedimentological and geochemical evidence shows that these climatic changes directly impacted the lake environment, e.g. through weaker thermal summer stratification (disappearance of the varves) and increased sedimentation rates. Simultaneously, we observe a cascade of changes in the pollen spectra, most likely reflecting both changes in pollen production by the present plant community as well as subsequent regional vegetation change (Fig. 2).

The term "YD" has been used to define a climatic event, to identify a lithostratigraphical, geochronological or biostratigraphical unit[5,25], and has been frequently conflated with Greenland Stadial-1[1]. Here, we use the term YD to indicate the youngest biostratigraphical LGIT zone characterised by the occurrence of sub-Arctic flora in northwest Europe. Biostratigraphical convention dictates that the onset of the YD biozone for large parts of Europe is defined as the midpoint of change in the LGIT pollen assemblages[12] toward a (sub-)arctic assemblage and is typically identified using community indicators such as a decrease in the total amount of Arboreal Pollen[12,16]. Similarly, the onset of the Holocene is defined by the midpoint of the increase in the total amount of Arboreal Pollen[12,16] as the pollen spectra shift toward a birch-pine forest assemblage. We refer to these definitions that use the midpoint of the biostratigraphical transition as the "*sensu stricto*" definitions, and apply this approach to the onset of both the YD and of the Holocene (YD_{SS} and HOL_{SS}). However, community response to environmental change will be the combined total of the individual species' responses and will therefore be both more gradual as well as delayed relative to the first changes observed in individual species records. Therefore, for each site we also determined the early onset of change, defined by the first change(s) in indicator taxa such as those at their distributional limits (YD_{early}/HOL_{early}). We determined the length of each biostratigraphical transition by calculating the interval

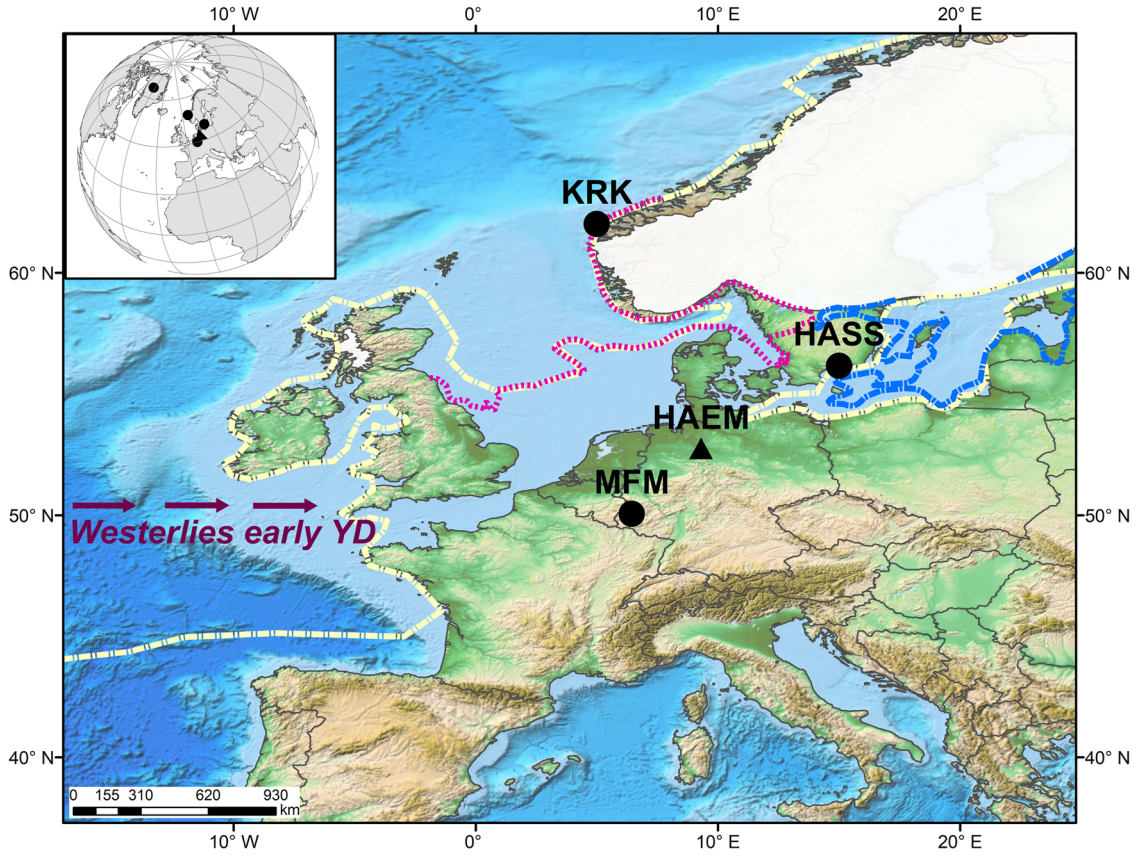

Fig. 1 YD palaeogeographic setting of northwest Europe. Hämelsee (triangle; HAEM) and other high-resolution palynological sites (circles; Kråkenes (KRK), Hässeldala Port (HASS), Meerfelder Maar (MFM)) are located on a N-S transect across northwest Europe. The maximum extent of the YD Scandinavian Ice sheet (white), the YD coastline of the North Sea (red line), the Baltic Ice Lake (blue line), and the winter sea ice extent (yellow line) are also shown[13,73].

between the early onset of change and the point at which a new equilibrium in the pollen spectra was reached (YD_{eq}/HOL_{eq}). The exact dates for the early onset of change and the date when new equilibrium was reached were determined visually as well as numerically using piecewise linear regression[26] (see Methods).

The first indications of vegetation change around lake Hämelsee (YD_{early}) can be identified at 12,820 (12,830–12,810) cal. yr BP or 185 years after the Laacher See eruption (Fig. 2; Supplementary Figs. 3 and 4; Supplementary Tables 2 and 3). Whilst arboreal taxa only show minor changes in their percent-abundances at this time, the Pollen Accumulation Rates (PARs) of e.g. *Salix* and *Juniperus* show a dramatic drop. The major decrease in *Betula* percent-abundances, typically used to identify the onset of the YD_{SS}, occurs at 12,800 (12,810–12,790) cal. yr BP, some 20 years after the first changes in the pollen spectra as identified in the Hämelsee record, but predating the end of varve-formation at 12,760 cal. yr BP. As the *Betula* pollen type likely includes pollen of tree birch (e.g. *P. pubescens*) as well as dwarf shrub (e.g. *B. nana*[27]), it is hard to attribute the decrease in *Betula* percent-abundances in the Hämelsee pollen record to a specific change in terrestrial vegetation. Subsequent drops in PAR (12,780 cal. yr BP) and the end of the decrease in *Betula* percent-abundances (12,755 cal. yr BP) predate the completion of the transition into the YD, which we identify as the end of the decrease in *Salix* and *Pinus* PARs at 12,730 (12,760–12,690) cal. yr BP. The full transition from an interstadial pollen assemblage to a stadial assemblage at lake Hämelsee lasted ca. 90 years.

The increase in heliophilous taxa (e.g. *Artemisia*) across the onset of the YD biozone indicates that terrestrial vegetation became more open as the pine-birch forest thinned[27,28]. This is additionally reflected in the µXRF record as a sharp decrease in the log(Fe/Ti) and log(Ca/Ti) signals as well as in the decreasing LOI values, indicating a change to an unstable catchment with increased sediment re-suspension and increased detrital sediment influx (Fig. 2).

We re-modelled the chronologies for three other northwest European sites that have high-resolution palynological datasets with closely constrained biostratigraphical boundaries (Meerfelder Maar, Hässeldala Port and Kråkenes). We use the latest radiocarbon calibration curve[29] and a tree-ring based radiocarbon-derived date for the LST[9] to improve the precision of dating at the onset of the YD at each of the sites. Our results show synchronous initial vegetation change (Figs. 3 and 4) for each of the sites on a N-S transect across northwest Europe (Fig. 1), within the resolution of the archives. At Meerfelder Maar, a decrease in PAR of, e.g., *Betula* (most likely *P. pubescens*[28]) and *Pinus* occurs at 155 years ± 40 after the LST (YD_{early}) and provides the first evidence of terrestrial ecosystem response to the onset of stadial conditions. At Hässeldala Port, *Empetrum* shows a decrease in percent-abundances at 12,865 (12,915–12,790) cal. yr BP (YD_{early}), and YD_{early} is observed at 12,820 (12,930–12,740) cal. yr BP at Kråkenes, suggesting synchronous (within multi-decadal dating uncertainties of the various models; Fig. 4) onset of vegetation change across northwest Europe. The dates for the onset of vegetation change in northwest Europe are slightly delayed when compared to the date for the onset of GS-1 in NGRIP when expressed on the IntCal20 timescale at 12,909 cal. yr BP (Fig. 3).

The age estimates for YD_{SS} for each of our sites show slightly larger variations. Whilst the YD_{SS} at both Hämelsee and MFM is

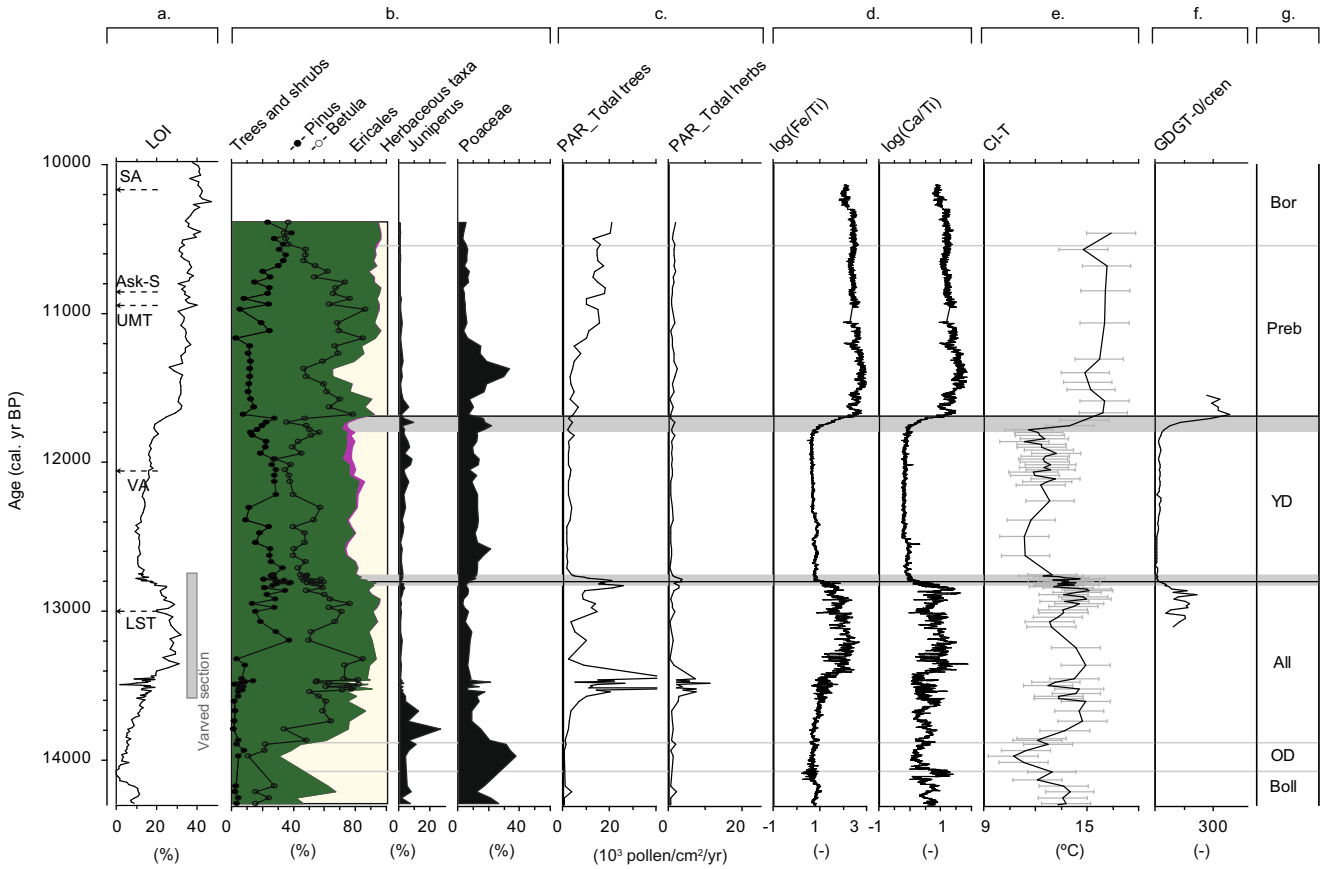

Fig. 2 High-resolution palaeoenvironmental data for the Haem13 lake Hämelsee record, indicating synchronous and abrupt changes in the palaeoenvironmental records at the onset of the YD and the Holocene. Chronological details and selected palaeoecological, geochemical and sedimentological data: **a** Loss-on-ignition record (see Supplementary Fig. 1 for a detailed lithological column), positions of tephra horizons (black; see Supplementary Table 1 for details) and varved sediment interval (grey); **b** Pollen percentages of selected taxa; **c** Pollen accumulation rates (PARs); **d** μXRF elemental ratios; **e** Chironomid-inferred July air temperature (CI-T) with sample-specific error estimates; **f** GDGT-0 / Crenarchaeol ratio as a proxy for windiness/lake mixing; **g** Biostratigraphical zonation follows the northwest European Late-Glacial zonation scheme[11]: Boll = Bølling, OD = Older Dryas, All = Allerød, YD = Younger Dryas, Preb = Preboreal, Bor = Boreal. Horizontal grey lines demarcate zonal boundaries, except at the onset and end of the YD, where the grey zones indicate the interval from the earliest changes observed in the pollen assemblages (YD_{early} and Hol_{early}, resp) to the point where a new state of equilibrium is reached (YD_{eq}, Hol_{eq}) with the black line indicating the location of the transitions sensu stricto (YD_{SS} and Hol_{SS}; see main text for more information).

dated to 12,800 (12,810–12,790) cal. yr BP or 205 years after the LST, estimates for Hässeldala and Kråkenes fall several decades later, at 12,755 (12,810–12,665) and 12,765 (12,840–12,700) cal. yr BP, respectively (Supplementary Table 2). Dates for the end of the transition vary more strongly, and, as a result, the duration of the YD transition varies between sites. The two German sites show abrupt transitions (duration 90–105 years) whereas the sites from Scandinavia show more gradual transitions (155–240 years; Fig. 4).

The pollen record of lake Hämelsee shows initial changes associated with Holocene climate warming from 11,790 (12,030–11,615) cal. yr BP onward, when PAR of *Empetrum* starts to decrease. The main change in the pollen diagram occurs 75 years later when *Betula* percent-abundances show an abrupt increase. The age estimates for the start of the transition into the Holocene vary notably between our sites, with the earliest start dated to 11,890 (11,970–11,805) cal. yr BP (Hässeldala) and the youngest to 11,640 ± 40 varve yr BP (MFM; Figs. 3 and 4). The dates for the onset of the Holocene *sensu stricto* vary between 11,740 and 11,520 cal. yr BP. The variable dates across the transition into the Holocene reflect larger uncertainties in the individual age/depth models, which result from the absence of precise chronological markers during this time interval. The non-linear nature of changes in some of the records additionally hampered the determination of points-of-change using numerical approaches (Supplementary Table 3). Nevertheless, it is clear that the duration of the YD/Holocene transition varies. It is relatively short at Hämelsee (100 years) and at MFM (50 years), whereas it is much longer at Hässeldala (220 years) and at Kråkenes (710 years). We hypothesise that factors such as migration speed, distance of refugia of thermophilic taxa and inter-species competition contributed to the more gradual nature of the transition in the Scandinavian sites[30].

Discussion

We observe that certain proxy records derived from the Haem13 sediment sequence show synchronous shifts at the early onset of the YD (e.g. pollen, GDGTs) whereas other records show a more delayed response when analysed at decadal timescales. These minor offsets most likely reflect site-specific differences in proxy sensitivity to climate forcing[31] or proxy-specific responses to changes to different parts of the local environment or different components of the climate system, such as aridification prior to cooling[19].

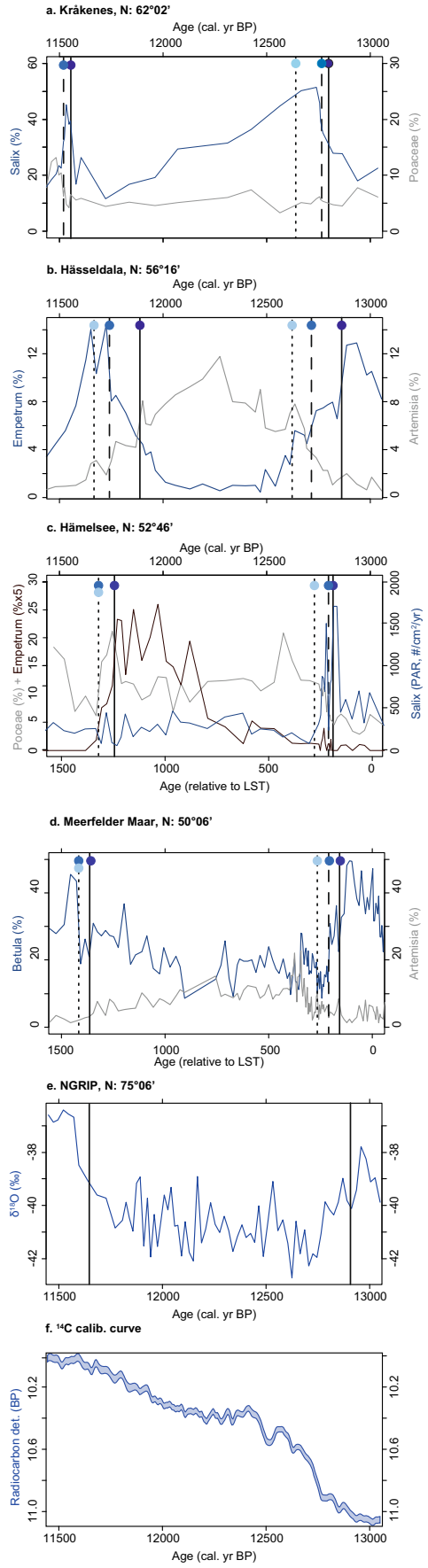

Fig. 3 Summary records of terrestrial ecosystem change for sites on a N-S transect across northwest Europe. Selected pollen taxa (%) are shown for **a** Kråkenes; **b** Hässeldala; **c** Hämelsee; **d** Meerfelder Maar. Solid vertical lines indicate the earliest onset of vegetation response to climate change (YD_{early} and HOL_{early} bold/ dark blue circle), dashed vertical lines (/blue circle) indicate the onset of the YD and Holocene sensu stricto (YD_{SS} and HOL_{SS}) and dotted lines (/light blue circle) the point where a new equilibrium was reached in the pollen spectra (YD_{eq} and HOL_{eq}). The **e** NGRIP $\delta^{18}O$ record[1] with vertical lines showing the onset and end of GS-1 and **f** IntCal20 radiocarbon calibration curve[29] are shown for comparison. All data are plotted on the IntCal20 timescale in cal. yr BP, except for the Meerfelder Maar record which is plotted in years relative to the LST datum (see Methods for more details).

Minor offsets, mostly not exceeding the dating uncertainties, also exist between the dates for the onset of vegetation change at each of the sites we have compared (Fig. 3). These offsets can be explained by differences in the sampling resolution for each of the records, by the uncertainties in the age/depth models, and by uncertainties related to proxy sensitivity.

The sites presented in Fig. 3 are among those from northwest Europe that combine the highest chronological precision and the highest-resolution palaeoenvironmental proxy analyses. However, many other late-glacial palynological records are available for mid-latitudinal Europe[32]. Re-evaluation of existing age/depth-models for further palynological sites across northwest Europe using the revised LST date[9] as well as the latest radiocarbon calibration curve[29] confirms the synchroneity of shifts in vegetation across the region (Supplementary Table 4) and suggests consistent immediate vegetation responses to regional climate change. For example, when considering the revised age for the LST, the timing of the onset of the YD biozone at sites in more easterly locations, such as Rehwiese (northeast Germany)[33], overlaps with the onset of the YD at Hämelsee. Similarly, recalibrated age-models for sites from the Netherlands suggest regional synchroneity in terrestrial ecosystem response at the onset of the YD across northwest Europe. By contrast, the onset of the YD at lake Gościąż (Poland) is later (12,620 cal. yr BP[31,34]) than observed at the sites reported here, but uncertainty estimates for the age/depth model of lake Gościąż are relatively large at +133/−231 year[35].

The four sites considered in this study show decadal-scale vegetation succession at the onset of the Holocene. However, the dates for the onset of the Holocene diverge between sites, likely reflecting the difficulties of dating the interval around 11,500 cal. yr BP. Only a few published sites have varve chronologies that span this critical climate transition[35,36] and radiocarbon dating is hampered by a plateau in the calibration curve[29] (Fig. 3). A recent application of ^{10}Be dating to an early Holocene interval of the MFM record[37] shows great potential for achieving increased chronological precision for early Holocene records, but the results do not yet extend to include the onset of the Holocene.

Vegetation adaptation to climate change at the onset of the Holocene shows complexity as different processes such as changes in pollen production by local vegetation, rapid colonisation and extra-regional migration interact with delayed permafrost melting[11]. More sites with a high density of age determinations and quasi-decadal pollen analyses across the YD/Holocene transition are needed to analyse the spatiotemporal complexity of vegetation change in Europe and beyond more robustly.

Ecosystem resilience theory suggests that poorly-competitive and slow self-replicating taxa are the first to disappear from a community under increased external stress[20,21]. When applied to

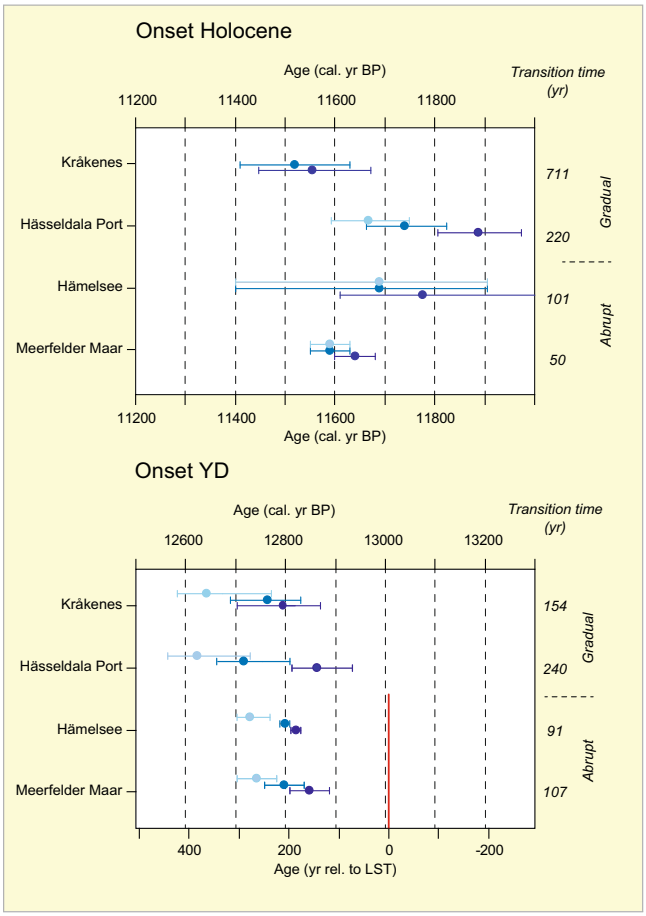

Fig. 4 Timing of the onset of the YD and the Holocene in high-resolution palynological sites. The onset of change for the YD and Holocene (dark blue), the date for the YD and Holocene onset sensu stricto (blue) and the end of the transitions (light blue) are given with 2-sigma uncertainty intervals. All dates are given in cal. yr BP except for the Meerfelder Maar ages for the onset of the YD, which are given relative to the LST, which is indicated by the solid red line. All records show a synchronous onset of the transition into the YD, with more abrupt transitions (shorter interval between YD_{early} and YD_{eq}) visible for the German sites. The dates for the onset of the Holocene are more variable, reflecting larger uncertainties in the individual age/depth models. Note that the date for HOL_{eq} at Kråkenes extends beyond the plotted time interval.

terrestrial vegetation these so-called 'canary species' could include those at the edge of their spatial distribution or those with competitive disadvantages. For example, in the lake Hämelsee record we observe that *Empetrum* acts as a canary species, declining in abundance several decades before the onset of the YD *sensu stricto* is observed. The different trends in *Empetrum* abundance between Hämelsee and, e.g., Hässeldala Port likely reflect differences in soil and nutrient conditions. This illustrates that whilst most sites will have canary species that react strongly to initial changes in, e.g., climate conditions, the controls on which species these will be and how they will behave, differ strongly from site to site. By contrast, strongly competitive 'keystone species' will be more resilient to external pressure and will only regress if pressure is sustained over longer periods or is of a greater amplitude[21,38].

Plants exhibit lower pollen production in situations of climatic stress[39], indicating that PAR records might be more sensitive indicators of changes in external drivers than pollen-percentage curves. We observe that for the Hämelsee and Meerfelder Maar records the arboreal PARs showed early and abrupt changes across the Allerød/YD transition. For instance, *Pinus* PARs decreased from ca. 8000 to 500 pollen cm^{-2} yr^{-1} between 12,790 and 12,710 cal. yr BP at lake Hämelsee. Whilst *Pinus* might not have immediately disappeared from the landscape, its pollen production decreased prior to the local extinction of the taxon. Similar results are shown for Den Treek (the Netherlands), where *Pinus* pollen production and its ability to set fruit, decreased at the onset of the YD, yet it took up to 70 years for pine to become locally extinct[40].

We therefore argue that for studies focussed on decadal-scale climate teleconnections, or on the determination of leads and lags in ecosystem response to climate change, the midpoint of change in a palaeoecological record is inappropriate. Instead, we suggest the identification of early changes in 'canary species', or a focus on parameters that are known to respond near-instantaneously to external drivers, such as PAR. Applying this approach to palynological records from lake Hämelsee as well as other key sites from Europe has shown that the start of the transition into the YD occurred several decades earlier than previously thought and indicates that previous suggestions of a north-south time-transgressive nature of vegetation change across Europe under LGIT cooling are no longer supported. The observed dates for the onset of the YD_{early} instead suggest that the impact of large-scale cooling was regionally synchronous across northwest Europe, arguing for abrupt and rapid vegetation response to climate forcing.

Methods

Site selection. Hämelsee was selected as our primary research focus due to its key location relative to climate drivers such as changes in North Atlantic circulation patterns and westerlies. Previous work on the site indicated the presence of at least two tephra horizons that could be used as chronological marker layers[27] and, given its location, there was the potential to identify additional tephra horizons. The presence of varved sediment intervals[27] furthermore indicated the potential to develop a robust chronological framework, and the relatively thick sediment interval dated to the LGIT allowed for the opportunity to study LGIT ecosystem change at high resolution. New sediment cores were retrieved from lake Hämelsee (north Germany) during fieldwork in 2013 and the composite record is referred to as Haem13 throughout this manuscript.

We provide a spatial context for the Hämelsee results by comparing them to palynological records from northwest Europe that were selected based on (a) their robust chronological control, utilising varve-counting, tephrochronology, or high-resolution radiocarbon dating (or a combination of these approaches); and (b) the presence of closely constrained biostratigraphic boundaries, together allowing the assessment of spatial differences in timing and duration of terrestrial ecosystem response. The additional lake sediment records were all obtained from small lacustrine basins located on a north-south transect across northwest Europe and have all previously been shown to respond sensitively to abrupt LGIT climate change[3,36,41].

Finally, we re-evaluated age-estimates for the Allerød/YD transition for sites across other parts of northwest Europe that did not meet the selection criteria described above. There is a very high number of sites available that cover the Allerød/YD transition in detail. For instance, the Neotoma database (https://apps.neotomadb.org/explorer) shows ca. 224 pollen records that contain the Allerød/YD transition for northwest Europe (accessed: 21/09/2021). As it is not possible to analyse such a high number of sites, the overview of sites included in Supplementary Table 4 is not comprehensive. Instead, we focussed on those sites that authors of this paper published on, for which we know a reliable date or age/depth model exists, and for which the chronological data is available publicly. Recalibrated radiocarbon ages are given as a 95% interval and are rounded to the nearest multiple of 5 years.

Chronological frameworks—palynological records. All of our comparison sites (Hämelsee, Meerfelder Maar, Hässeldala and Kråkenes) have detailed chronological frameworks allowing for the precise determination of the onset and end of the YD. The age/depth-models are based on AMS radiocarbon (^{14}C) dating, varve counting and tephrochronology or a combination of these methods. We present an age/depth model for the Haem13 core from lake Hämelsee. We additionally make several revisions to the existing age/depth models for the other sites to enhance their accuracy and precision, allowing for a robust comparison of palynological changes observed in the individual records.

Hämelsee. A detailed cryptotephra investigation revealed the presence of eight tephra horizons in the LGIT and early Holocene sediment interval of the

Haem13 sequence from lake Hämelsee[22]. Five of the tephra layers could be reliably correlated to known eruptions with published independent age estimates established from radiocarbon dating programmes at other sites, which were here updated using the IntCal20 calibration curve[29] (Supplementary Table 2; Supplementary Methods 1). Five samples were selected for AMS ^{14}C dating from those parts of the Hämelsee record where no tephra horizons were available. Organic material reflecting atmospheric ^{14}C concentrations such as seeds and fruits from terrestrial plants were hand-picked from the residue left after sieving, and dated in the Oxford Radiocarbon Accelerator Unit (Supplementary Table 2). A varve chronology has been established for an annually laminated sediment interval (1610–1524 cm sediment depth) based on counting and sub-layer thickness measurements on 10-cm-long thin sections using a petrographic microscope. The floating varve chronology is anchored to the absolute timescale using the LST identified between 1559 and 1557 cm depth[22]. The varve chronology presented here includes a total number of 825 ± 5 varves—with the uncertainty estimate derived from replicate counts by two independent examiners. A Bayesian age-depth (depositional) model, "HaemChron21", was constructed for the LGIT section of the Hämelsee record in OxCal v4.4[42]. To allow for the range of age controls, three connected *P_Sequence* model segments were run, applying outlier analysis, to interpolate through: i. the Younger Dryas to Holocene section of the record from 1524.5 – 1370 cm, constrained with both ^{14}C and tephra age estimates; ii. the Allerød into Younger Dryas floating varve section between 1610–1524.5 cm, with varve ages calculated relative to the dated LST anchor point; and iii. the base of the sequence at 1696 cm to the start of the varve sequence at 1610 cm depth, constrained only by ^{14}C age estimates. Using the OxCal outlier analysis function, one radiocarbon date was excluded from (down-weighted to a probability of 0) the lowermost *P_Sequence* model, due to the apparent inclusion of young carbon in a very small sample. All radiocarbon dates in the model were calibrated using the IntCal20 calibration curve[29]. Uncertainties for varve ages combine the estimated varve counting uncertainty (± 4 varves) with the uncertainty estimate for the LST anchor point (± 4.5 years at 1 sigma[9], rounded to ± 5 in the model). The full HaemChron21 OxCal code is included in Supplementary Code 1.

Hässeldala and Kråkenes. Lake Kråkenes[41,43,44] and lake Hässeldala[13,45] are key sites in southern Scandinavia that combine a robust chronology with a range of sedimentological and palaeoecological data to infer past climate and landscape change across the LGIT. The existing age/depth models of lake Kråkenes and lake Hässeldala are based on 118 and 49 AMS radiocarbon dates, respectively (Supplementary Table 5). Bayesian modelling and the IntCal13 calibration curve were used to develop the original age/depth models and here we re-ran the original age/depth models using the latest IntCal20 calibration curve to provide the most accurate age estimates possible. The age/depth models for lake Kråkenes and lake Hässeldala have been developed using OxCal v4.4[42], and OxCal code can be accessed through the original publications (see Supplementary Table 5).

Meerfelder Maar. Large parts of the Holocene and LGIT intervals in the sediment record of lake Meerfelder Maar are varved, and MFM is one of only three lakes known in Europe with continuous annually laminated sediments preserved throughout most of the Younger Dryas[36,46]. Human impact prevented varve preservation in the youngest part of the record, and the floating MFM varve chronology has been anchored to the absolute timescale using the Ulmener Maar Tephra which has itself been varve-dated using the continuously laminated sediment sequence from nearby lake Holzmaar[36]. This approach resulted in an age-estimate for the Vedde Ash of 12,140 ± 40 varve yr BP[47], which overlaps with a radiocarbon-based modelled age estimate for the Vedde Ash of 12,102–11,914 cal. yr BP (95% range)[48] and the GICC05 age of the Vedde Ash located in the NGRIP ice core, of 12,121 ± 114 yr BP (converted from b2k)[49]. However, the MFM varve-based age estimate for the LST is 12,880 ± 40 varve yr BP, which is significantly younger than an age estimate of 13,006 ± 9 cal. yr BP established through dendrochronological analysis and ^{14}C dating of tree trunks buried in the LST[9]. In our study we use the LST age of 13,006 ± 9 cal. yr BP[9], rather than the age from the MFM study, in the construction of the HaemChron21 chronology, as we believe that it represents the most robust age for the tephra layer published to date. In support of the dendrochronologically determined age[9] we note that it is in line with an estimate of the LST age based on the ^{14}C dates bracketing the LST in the MFM sequence[50]. A Bayesian *P_Sequence* model of the LST age using the radiocarbon dates and depth information from the 1996 MFM sequence provides an age estimate of 13,017 ± 129 cal. yr BP (68% range; this study).

The MFM varve chronology suggests that ca. 740 varves occur between the LST and the Vedde Ash (in contrast to ~900 years in the HaemChron21 chronology) and assuming that the two tephra layers are preserved in-situ, we therefore meet a problem in comparing the two archives based on their own chronologies. Adjusting the entire MFM varve-chronology in a linear fashion, using the dendrochronological LST age determination[9] would lead to erroneous dates for the Vedde Ash and would suggest the existence of a hiatus in the MFM sequence, which is not supported by any sedimentological evidence. In fact, there is excellent replication of MFM's ~200 varve year interval between the LST – YD onset, reported from a suite of varved lake sediment sequence in Germany and Poland[51]. The consistency of the 200 year interval suggests that the origin of the offset between Meerfelder Maar and Hämelsee chronologies falls within the first half of the Younger Dryas. Therefore, to avoid re-calculating the age model for MFM without secure evidence for any mode of adjustment, we here report the ages of changes in the pollen spectra of MFM relative to the age of the LST (set as a datum: LST = year 0) for the interval covering the Allerød/YD transition (Figs. 3; 4). A reliable error estimate is difficult to determine for this interval, and we here use the previously reported age uncertainty of ± 40 yr for the entire MFM sequence[52,53].

Chronological frameworks—Greenland ice core records. To compare the timing of events recorded in Greenland ice cores and radiocarbon dated records, we synchronised the GICC05 and IntCal20 timescales using the Bayesian wiggle matching approach[54,55]. The method relies on wiggle matching periodic short-term solar modulations integrated in GRIP and GISP2 ^{10}Be flux (on the GICC05 timescale) to Δ^{14}C estimates inferred from IntCal20 over the interval 11.5–13.5 ka[56]. The ^{10}Be data were initially stacked and converted to Δ^{14}C variations using a Box-Diffusion carbon-cycle model[57] initialised with pre-industrial boundary conditions assuming a constant carbon cycle. Prior to wiggle matching, the ^{10}Be-based and IntCal Δ^{14}C records were bandpass filtered between cut-off frequencies of 1/100 and 1/500 years to focus on the common solar-induced centennial changes in cosmogenic production rates. Bayesian wiggle matching was performed on the filtered data using moving time windows of 1000 years length at 20-year time steps, which allowed estimates for leads/lags within ±150 years applied to the ice core timescales relative to IntCal20. The probabilities of each individual lead-lag measurement were combined to obtain an overall timescale shift likelihood at each time step between GICC05 and IntCal20. The results show that, e.g., the onset of GS-1 in NGRIP is 12,846 yr (before 1950) when expressed on the GICC05 timescale, and changes to 12,909 cal. yr BP when expressed on the IntCal20 timescale. The estimated timescale offsets are well within the stated uncertainties of the ice core timescales (Supplementary Fig. 5) and in good agreement with previous results[55,58,59].

Hämelsee—pollen record. Palynological records allow for a detailed reconstruction of vegetation response to external forcing and, among other things, provide information on local to regional-scale vegetation change[15]. Here we provide new palynological results with a sub-decadal scale resolution across the major LGIT transitions for lake Hämelsee.

Pollen samples were prepared for the Haem13 cores retrieved in 2013 following standard procedures[60], as described in detail in Engels et al.[16]. Contiguous 1-cm-thick samples were selected across the major transitions visible in the sedimentological records of the core, with additional pollen samples evenly distributed across the other core sections. The final pollen record for lake Hämelsee includes 105 samples (Supplementary Fig. 3; Supplementary Table 5), and the results are expressed as a percentage of the total pollen sum which includes trees, shrubs and upland herbaceous taxa. Cyperaceae were excluded from the pollen sum which averaged 472 pollen grains per sample (range: 307–849 pollen grains). The dataset of pollen counts is available on PANGAEA[61].

Pollen accumulation rates (PARs) were additionally calculated for selected taxa by first multiplying the number of encountered pollen grains by the ratio of the number of added *Lycopodium* spores relative to the number of spores encountered during the analysis. The resulting number was then corrected for the surface area of the pollen sample and the number of years included in each sample (as derived from the age/depth model). PARs are presented as the number of palynomorphs cm^{-2} $year^{-1}$.

Hämelsee—other proxy indicators. The geochemical composition of the sediments was determined on freshly split core sections using an Itrax X-ray fluorescence (XRF) core scanner equipped with a Cr tube. Measurements were performed at 200 µm resolution during 20 s exposure time per step at 30 kV tube voltage and 40 mA tube current. The selected geochemical elements (Ti, Ca, Fe) are expressed as log ratio (Log) to reduce matrix effects[62]. We report here on the log(Fe/Ti) and the log(Ca/Ti) ratios which we interpret to represent conditions around and within the lake, with more negative ratios indicative of dynamic conditions, and more positive ratios of more stable catchment and lake conditions[36].

Loss-on-ignition was determined for consecutive 1-cm-thick samples across the entire Late-Glacial and early Holocene period and for both core sequences recovered from the lake during fieldwork in 2013. The LOI curve presented here reflects all samples that are part of the Haem13 composite record, spanning 1695–1321 cm core depth (369 samples representing a decadal-scale sampling resolution). Volumetric samples (1 cm^3) where dried in an oven at 105 °C before being placed in a furnace at 550 °C for 4 h. Loss-on-ignition was calculated by comparing the weight of the sample before and after combustion at 550 °C and expressed as a percentage[63].

A total of 123 samples were analysed for subfossil chironomid remains and were prepared following standard procedures[64]. Chironomid head capsules were identified using Brooks et al.[64] and the dataset presented here has been matched to the taxonomy of the merged Norwegian/Swiss chironomid-climate calibration dataset[65]. This means that specimens that could not be identified beyond subfamily or tribe level due to, e.g., missing mouth parts were excluded from the final dataset, as were a small number of rare taxa that were present in the fossil dataset but absent from the calibration dataset (e.g. *Propsilocerus lacustris*-type). As several samples had low chironomid concentrations and sediment availability was limited, we amalgamated adjacent samples (within lithological boundaries) with the aim of reaching a minimum count sum of 50 head capsules per sample[66]. Our final chironomid dataset contains 97 samples with an average count sum of 83 head

capsules (range: 50.5–214.5). As temperature was believed to be the primary driver of changes in the fossil dataset, a combined Norwegian-Swiss dataset[65], consisting of 274 lakes, was used to quantitatively infer past July air temperatures (T_{jul}) from the chironomid data. As many of the fossil specimens of the genus *Paratanytarsus* were missing mouthparts essential for identification beyond genus level, we amalgamated the taxa *P. austriacus*-type and *P. penicillatus*-type as included in the calibration dataset to the generic taxon *Paratanytarsus* spp. The reconstruction is based on a 2-component weighted averaging-partial least squares (WA-PLS) regression model, with outliers (as specified in the original publication) removed prior to analysis. The inference model has a cross-validated (1000 bootstrap cycles) r^2_{boot} of observed versus predicted temperatures of 0.86, a root-mean-squared error of prediction of 1.46 °C and a maximum bias of 0.95 °C. Sample specific error estimates were calculated using bootstrapping (999 cycles).

A total of 94 samples were processed using a Dionex 350 accelerated solvent extraction (ASE) system. The extracts were separated into an aliphatic, aromatic and alcohol/fatty acid fraction by solid phase extraction (SPE) using the manual method described in Rach et al.[67]. In brief, this was achieved by loading the extracts on activated silica columns and eluting the samples successively with hexane, hexane/DCM (4:1 v/v) and DCM/MeOH (9:1 v/v) for each fraction, respectively. To analyse the glycerol dialkyl glycerol tetraether lipid content, a known amount of C_{46} GTGT standard was added to the alcohol/fatty acid fraction of the extracts before measurement[68]. The fraction was then dried under N_2, redissolved in hexane:isopropanol (99:1) and passed over a 0.45 µm PTFE filter prior to analysis with an Agilent 1260 Infinity ultra-high performance liquid chromatograph (UHPLC) coupled to an Agilent 6130 single quadrupole mass spectrometer (MS), with source settings according to Hopmans et al.[69]. The GDGTs were separated over two silica Waters Acquity UPLC BEH HILIC columns (1.7 µm, 2.1 mm × 150 mm) held at 30 °C, preceded by a guard column packed with the same material. The GDGTs were eluted isocratically for 25 min using 82% hexane (A) and 18% hexane:isopropanol (99:1) (B), followed by a linear gradient to 70% A and 30% B for 25 min, and then to 0% A and 100% B in 30 min with a constant flow rate of 0.2 ml/min. Single ion monitoring of the $[M + H]^+$ ions was used to detect the GDGTs. Quantification was achieved by comparing the peak area of each GDGT to that of the internal standard, thereby assuming equal response of the MS for the GDGTs and the internal standard.

We calculated the GDGT-0/Crenarchaeol ratio which we use as an indicator of lake water oxygenation and/or windiness. High values of GDGT-0/Crenarchaeol (i.e., higher than 2.0) in lake ecosystems are often associated with relatively high abundances of methanogenic Euryarchaeota[23,24]. A state with increased contributions from methanogens is typically linked to lower levels of oxygen in the lake water related to reduced mixing of the water column.

Northwest European pollen records. Whilst a high-resolution pollen-record was already available for lake Meerfelder Maar[28], a recent study[16] increased the sampling resolution across the Allerød/Younger Dryas transition to infer in high detail vegetation changes during this time interval. As taxonomical differences between the different datasets were very minor, we created a composite LGIT pollen record for Meerfelder Maar containing the Allerød/YD samples of Engels et al.[16] and the mid-to late-YD samples from Litt & Stebich[28]. (Supplementary Table 5). The final dataset consists of 163 samples and has an average sampling resolution of 15 yr $sample^{-1}$.

We used the originally published dataset for Hässeldala[3], as well as an updated version of the Kråkenes dataset[41], which has an increased sampling resolution across the transition zones[44,70]. More details for each dataset are provided in Supplementary Table 5.

Palynological sampling resolution differs between our selected sites. The Hämelsee, Hässeldala and Kråkenes records have an average sampling density of 35–60 years per pollen sample (Supplementary Table 5) although increased sampling resolutions around the LGIT transitions mean that for these parts sampling density generally is higher at 20–40 yr per sample (Supplementary Table 5). The Meerfelder Maar record has a much higher number of pollen samples, allowing for sub-decadal analysis of vegetation change during the transitional periods.

Determination of points-of-change. In the first instance, the datasets were checked visually to identify 'canary species' as well as the early, *sensu stricto* and equilibrium dates in the selected records (see Supplementary Table 2 for results). We applied piecewise linear regression (PLR) to these selected taxa to verify our visual interpretation by analysing the data using the segmented package[26] in R[71]. We provide the R code in Supplementary Code 2. Aside from climate, drivers of the terrestrial flora varied based on time-interval and site. For instance, at Meerfelder Maar there were indications of the effects of the Laacher See eruption on the local vegetation ca. 200 yr prior to the onset of the YD[72], whereas in Kråkenes delayed vegetation response to climate warming at the onset of the Holocene resulted from processes such as the migration lag of tree birch[41]. We therefore selected bespoke time intervals for each run in R and report the results in Supplementary Table 3, where we show that in 10 of 16 instances (63%) the results between visual establishment of boundaries and statistical analyses were identical (here defined as breakpoints falling between the same pair of datapoints). For another 4 instances, the difference between the visually established transition and the PLR result was only one or two samples (25%), i.e. of a decadal scale. The latter was most likely due to the fact that PLR assumes linear trends exist in the data, whereas in reality the transitions at times showed a more gradual onset of change followed by a more abrupt transition; in these cases, PLR struggled to pick up the earliest point of change. In only 2 instances PLR was not able to establish points of change, which was most likely due to a combination of low data resolution and a non-linear trend in these records. To ensure consistency, we report the visually established transition dates (Supplementary Table 2) in the manuscript.

Data availability

The pollen data generated for the Haem13 cores that support the findings of this study are available in the PANGAEA repository (PDI-939693).

Code availability

The HaemChron21 OxCal code is included in Supplementary Code 1. The R code used for point-of-change estimation is included in Supplementary Code 2.

Received: 23 December 2021; Accepted: 13 May 2022;
Published online: 09 June 2022

References

1. Rasmussen, S. O. et al. A stratigraphic framework for abrupt climatic changes during the Last Glacial period based on three synchronized Greenland ice-core records: refining and extending the INTIMATE event stratigraphy. *Quat. Sci. Rev.* **106**, 14–28 (2014).
2. Heiri, O. et al. Validation of climate model-inferred regional temperature change for late-glacial Europe. *Nat. Commun.* **5**, 1–7 (2014).
3. Muschitiello, F. et al. Fennoscandian freshwater control on Greenland hydroclimate shifts at the onset of the Younger Dryas. *Nat. Commun.* **6**, 1–8 (2015).
4. Renssen, H. et al. Multiple causes of the Younger Dryas cold period. *Nat. Geosci.* **8**, 946–949 (2015).
5. Mangerud, J. The discovery of the Younger Dryas, and comments on the current meaning and usage of the term. *Boreas* **50**, 1–5 (2021).
6. Cheng, H. et al. Timing and structure of the Younger Dryas event and its underlying climate dynamics. *Proc. Natl. Acad. Sci. USA* **117**, 23408–23417 (2020).
7. van Hoesel, A., Hoek, W. Z., Pennock, G. M. & Drury, M. R. The Younger Dryas impact hypothesis: a critical review. *Quat. Sci. Rev.* **83**, 95–114 (2014).
8. Partin, J. W. et al. Gradual onset and recovery of the Younger Dryas abrupt climate event in the tropics. *Nat. Commun.* **6**, 1–9 (2015).
9. Reinig, F. et al. Precise date for the Laacher See eruption synchronizes the Younger Dryas. *Nature* **595**, 66–69 (2021).
10. Ammann, B. et al. Quantification of biotic responses to rapid climatic changes around the Younger Dryas — a synthesis. *Palaeogeogr. Palaeoclimatol. Palaeoecol.* **159**, 313–347 (2000).
11. Hoek, W. Z. Vegetation response to the ~ 14.7 and ~ 11.5 ka cal. BP climate transitions: is vegetation lagging climate? *Glob. Planet. Change* **30**, 103–115 (2001).
12. Litt, T. et al. Correlation and synchronisation of Lateglacial continental sequences in northern central Europe based on annually laminated lacustrine sediments. *Quat. Sci. Rev.* **20**, 1233–1249 (2001).
13. Muschitiello, F. & Wohlfarth, B. Time-transgressive environmental shifts across Northern Europe at the onset of the Younger Dryas. *Quat. Sci. Rev.* **109**, 49–56 (2015).
14. Nakagawa, T. et al. The spatio-temporal structure of the Lateglacial to early Holocene transition reconstructed from the pollen record of Lake Suigetsu and its precise correlation with other key global archives: implications for palaeoclimatology and archaeology. *Glob. Planet. Change* **202**, 103493 (2021).
15. Ammann, B. et al. Vegetation responses to rapid warming and to minor climatic fluctuations during the Late-Glacial Interstadial (GI-1) at Gerzensee (Switzerland). *Palaeogeogr. Palaeoclimatol. Palaeoecol.* **391**, 40–59 (2013).
16. Engels, S. et al. Subdecadal-scale vegetation responses to a previously unknown late-Allerød climate fluctuation and Younger Dryas cooling at Lake Meerfelder Maar (Germany). *J. Quat. Sci* **31**, 741–752 (2016).
17. Van Raden, U. J. et al. High-resolution late-glacial chronology for the Gerzensee lake record (Switzerland): δ18O correlation between a Gerzensee-stack and NGRIP. *Palaeogeogr. Palaeoclimatol. Palaeoecol.* **391**, 13–24 (2013).
18. Blaga, C. I., Reichart, G.-J., Lotter, A. F., Anselmetti, F. S. & Sinninghe Damsté, J. S. A TEX86 lake record suggests simultaneous shifts in temperature in Central Europe and Greenland during the last deglaciation. *Geophys. Res. Lett.* **40**, 948–953 (2013).

19. Rach, O., Brauer, A., Wilkes, H. & Sachse, D. Delayed hydrological response to Greenland cooling at the onset of the Younger Dryas in western Europe. *Nat. Geosci.* **7**, 109 (2014).
20. Strogatz, S. H. Exploring complex networks. *Nature* **410**, 268–276 (2001).
21. Doncaster, C. P. et al. Early warning of critical transitions in biodiversity from compositional disorder. *Ecology* **97**, 3079–3090 (2016).
22. Jones, G. et al. The Lateglacial to early Holocene tephrochronological record from Lake Hämelsee, Germany: a key site within the European tephra framework. *Boreas* **47**, 28–40 (2018).
23. Blaga, C. I., Reichart, G.-J., Heiri, O. & Damsté, J. S. S. Tetraether membrane lipid distributions in water-column particulate matter and sediments: a study of 47 European lakes along a north–south transect. *J. Paleolimnol.* **41**, 523–540 (2009).
24. Bechtel, A., Smittenberg, R. H., Bernasconi, S. M. & Schubert, C. J. Distribution of branched and isoprenoid tetraether lipids in an oligotrophic and a eutrophic Swiss lake: insights into sources and GDGT-based proxies. *Org. Geochem.* **41**, 822–832 (2010).
25. Lowe, J. et al. On the timing of retreat of the Loch Lomond ('Younger Dryas') Readvance icefield in the SW Scottish Highlands and its wider significance. *Quat. Sci. Rev.* **219**, 171–186 (2019).
26. Muggeo, V. M. R. Segmented: an R package to fit regression models with broken-line relationships. *R news* **8**, 20–25 (2008).
27. Merkt, J. & Müller, H. Varve chronology and palynology of the Lateglacial in Northwest Germany from lacustrine sediments of Hämelsee in Lower Saxony. *Quat. Int.* **61**, 41–59 (1999).
28. Litt, T. & Stebich, M. Bio-and chronostratigraphy of the lateglacial in the Eifel region, Germany. *Quat. Int.* **61**, 5–16 (1999).
29. Reimer, P. J. et al. The IntCal20 Northern hemisphere radiocarbon age calibration curve (0–55 cal kBP). *Radiocarbon* **62**, 725–757 (2020).
30. Giesecke, T. Holocene dynamics of the southern boreal forest in Sweden. *The Holocene* **15**, 858–872 (2005).
31. Müller, D. et al. New insights into lake responses to rapid climate change: the Younger Dryas in Lake Gościąż, central Poland. *Boreas* **50**, 535–555 (2021).
32. Davis, B. A. S. et al. The Eurasian Modern Pollen Database (EMPD), version 2. *Earth Syst. Sci. data* **12**, 2423–2445 (2020).
33. Neugebauer, I. et al. A Younger Dryas varve chronology from the Rehwiese palaeolake record in NE-Germany. *Quat. Sci. Rev.* **36**, 91–102 (2012).
34. Ralska-Jasiewiczowa, M. et al. Very fast environmental changes at the Pleistocene/Holocene boundary, recorded in laminated sediments of Lake Gościąż, Poland. *Palaeogeogr. Palaeoclimatol. Palaeoecol.* **193**, 225–247 (2003).
35. Bonk, A. et al. Varve microfacies and chronology from a new sediment record of Lake Gościąż (Poland). *Quat. Sci. Rev.* **251**, 106715 (2021).
36. Brauer, A., Haug, G. H., Dulski, P., Sigman, D. M. & Negendank, J. F. W. An abrupt wind shift in western Europe at the onset of the Younger Dryas cold period. *Nat. Geosci.* **1**, 520–523 (2008).
37. Mekhaldi, F. et al. Radionuclide wiggle matching reveals a nonsynchronous early Holocene climate oscillation in Greenland and western Europe around a grand solar minimum. *Clim. Past* **16**, 1145–1157 (2020).
38. Mayfield, R. J. et al. Metrics of structural change as indicators of chironomid community stability in high latitude lakes. *Quat. Sci. Rev.* **249**, 106594 (2020).
39. van der Knaap, W. O. & Van Leeuwen, J. F. N. Climate-pollen relationships AD 1901–1996 in two small mires near the forest limit in the northern and central Swiss Alps. *The Holocene* **13**, 809–828 (2003).
40. Bazelmans, J. et al. Environmental changes in the late Allerød and early Younger Dryas in the Netherlands: a multiproxy high-resolution record from a site with two Pinus sylvestris populations. *Quat. Sci. Rev.* **272**, 107199 (2021).
41. Birks, H. H., Battarbee, R. W. & Birks, H. J. B. The development of the aquatic ecosystem at Kråkenes Lake, western Norway, during the late glacial and early Holocene-a synthesis. *J. Paleolimnol* **23**, 91–114 (2000).
42. Bronk Ramsey, C. Bayesian analysis of radiocarbon dates. *Radiocarbon* **51**, 337–360 (2009).
43. Lohne, Ø. S., Mangerud, J. A. N. & Birks, H. H. IntCal13 calibrated ages of the Vedde and Saksunarvatn ashes and the Younger Dryas boundaries from Kråkenes, western Norway. *J. Quat. Sci* **29**, 506–507 (2014).
44. Lohne, Ø. S., Mangerud, J. A. N. & Birks, H. H. Precise 14 C ages of the Vedde and Saksunarvatn ashes and the Younger Dryas boundaries from western Norway and their comparison with the Greenland Ice Core (GICC 05) chronology. *J. Quat. Sci* **28**, 490–500 (2013).
45. Wohlfarth, B. et al. Hässeldala–a key site for last termination climate events in northern Europe. *Boreas* **46**, 143–161 (2017).
46. Brauer, A. et al. High resolution sediment and vegetation responses to Younger Dryas climate change in varved lake sediments from Meerfelder Maar, Germany. *Quat. Sci. Rev.* **18**, 321–329 (1999).
47. Lane, C. S., Brauer, A., Blockley, S. P. E. & Dulski, P. Volcanic ash reveals time-transgressive abrupt climate change during the Younger Dryas. *Geology* **41**, 1251–1254 (2013).
48. Bronk Ramsey, C. et al. Improved age estimates for key Late Quaternary European tephra horizons in the RESET lattice. *Quat. Sci. Rev.* **118**, 18–32 (2015).
49. Rasmussen, S. O. et al. A new Greenland ice core chronology for the last glacial termination. *J. Geophys. Res. Atmos.* **111**, https://doi.org/10.1029/2005JD006079 (2006).
50. Brauer, A., Endres, C., Zolitschka, B. & Negendank, J. F. W. AMS radiocarbon and varve chronology from the annually laminated sediment record of Lake Meerfelder Maar, Germany. *Radiocarbon* **42**, 355–368 (2000).
51. Wulf, S. et al. Tracing the Laacher See Tephra in the varved sediment record of the Trzechowskie palaeolake in central Northern Poland. *Quat. Sci. Rev.* **76**, 129–139 (2013).
52. Brauer, A. et al. The importance of independent chronology in integrating records of past climate change for the 60–8 ka INTIMATE time interval. *Quat. Sci. Rev.* **106**, 47–66 (2014).
53. Lane, C. S. et al. The Late Quaternary tephrostratigraphy of annually laminated sediments from Meerfelder Maar, Germany. *Quat. Sci. Rev.* **122** 192–206 (2015).
54. Adolphi, F. & Muscheler, R. Synchronizing the Greenland ice core and radiocarbon timescales over the Holocene–Bayesian wiggle-matching of cosmogenic radionuclide records. *Clim. Past* **12**, 15–30 (2016).
55. Muschitiello, F. et al. Deep-water circulation changes lead North Atlantic climate during deglaciation. *Nat. Commun.* **10**, 1–10 (2019).
56. Adolphi, F. et al. Persistent link between solar activity and Greenland climate during the Last Glacial Maximum. *Nat. Geosci.* **7**, 662–666 (2014).
57. Siegenthaler, U., Heimann, M. & Oeschger, H. 14C variations caused by changes in the global carbon cycle. *Radiocarbon* **22**, 177–191 (1980).
58. Muscheler, R., Adolphi, F. & Svensson, A. Challenges in 14C dating towards the limit of the method inferred from anchoring a floating tree ring radiocarbon chronology to ice core records around the Laschamp geomagnetic field minimum. *Earth Planet. Sci. Lett.* **394**, 209–215 (2014).
59. Muschitiello, F. An improved and continuous synchronization of the Greenland ice-core and Hulu Cave U-Th timescales using probabilistic inversion. *Clim. Past Discuss.* 1–39 https://doi.org/10.5194/cp-2021-116 (2021).
60. Moore, P. D., Webb, J. A. & Collison, M. E. *Pollen analysis*. (Blackwell scientific publications, 1991).
61. Engels, S. et al. Haemelsee: late-glacial pollen counts. PANGAEA, https://doi.org/10.1594/PANGAEA.939693 (2021).
62. Weltje, G. J. & Tjallingii, R. Calibration of XRF core scanners for quantitative geochemical logging of sediment cores: Theory and application. *Earth Planet. Sci. Lett.* **274**, 423–438 (2008).
63. Heiri, O., Lotter, A. F. & Lemcke, G. Loss on ignition as a method for estimating organic and carbonate content in sediments: reproducibility and comparability of results. *J. Paleolimnol* **25**, 101–110 (2001).
64. Brooks, S. J., Langdon, P. G. & Heiri, O. The identification and use of Palaearctic Chironomidae larvae in palaeoecology. *Quat. Res. Assoc. Tech. Guid.* i–vi. Vol. 10, 1–276 (2007).
65. Heiri, O., Brooks, S. J., Birks, H. J. B. & Lotter, A. F. A 274-lake calibration data-set and inference model for chironomid-based summer air temperature reconstruction in Europe. *Quat. Sci. Rev.* **30**, 3445–3456 (2011).
66. Heiri, O. & Lotter, A. F. Effect of low count sums on quantitative environmental reconstructions: an example using subfossil chironomids. *J. Paleolimnol* **26**, 343–350 (2001).
67. Rach, O., Hadeen, X. & Sachse, D. An automated solid phase extraction procedure for lipid biomarker purification and stable isotope analysis. *Org. Geochem.* **142**, 103995 (2020).
68. Huguet, C. et al. An improved method to determine the absolute abundance of glycerol dibiphytanyl glycerol tetraether lipids. *Org. Geochem.* **37**, 1036–1041 (2006).
69. Hopmans, E. C., Schouten, S. & Damsté, J. S. S. The effect of improved chromatography on GDGT-based palaeoproxies. *Org. Geochem.* **93**, 1–6 (2016).
70. Birks, H. J. B. & Birks, H. H. Biological responses to rapid climate change at the Younger Dryas—Holocene transition at Kråkenes, western Norway. *The Holocene* **18**, 19–30 (2008).
71. R CORE TEAM, A. R: A language and environment for statistical computing. R Foundation for Statistical Computing, Vienna, Austria. 2012. URL http://www.R-project.org (2020).
72. Engels, S., van Geel, B., Buddelmeijer, N. & Brauer, A. High-resolution palynological evidence for vegetation response to the Laacher See eruption from the varved record of Meerfelder Maar (Germany) and other central European records. *Rev. Palaeobot. Palynol.* **221**, 160–170 (2015).
73. Hughes, A. L. C., Gyllencreutz, R., Lohne, Ø. S., Mangerud, J. & Svendsen, J. I. The last Eurasian ice sheets–a chronological database and time-slice reconstruction, DATED-1. *Boreas* **45**, 1–45 (2016).

Acknowledgements

This study makes a contribution to the INTIMATE project (INTegrating Ice core, MArine and TErrestrial records, http://intimate.nbi.ku.dk/) and follows on from the INTIMATE Example 2013 Research and Training school, which was funded by COST action ES0907. We thank all of the participants in the INTIMATE Example 2013 training school for their contribution to this research, as well as Camping Rittergut Hämelsee and the coring team. We thank Hilary and John Birks for providing the pollen data from lake Kråkenes for comparison and Achim Brauer and Dirk Sachse for supporting laboratory analyses and for providing helpful comments on a previous draft of the manuscript.

Author contributions

S.E., C.L. and W.H. designed and coordinated the research. S.E., C.L., F.M., W.H., I.B., A.Bo, C.B.R., J.C., Rd.B., A.H., O.H., K.H., G.J., A.L., J.M., M.M., T.P., F.P., R.S., At.S., F.T., V.vdB. and F.W.C. acquired, analysed and interpreted the data. S.E. wrote the first draft of the manuscript and all authors contributed to editing the paper.

Competing interests

The authors declare no competing interests.

Additional information

Supplementary information The online version contains supplementary material available at https://doi.org/10.1038/s43247-022-00457-y.

Correspondence and requests for materials should be addressed to Stefan Engels.

Peer review information *Communications Earth & Environment* thanks Sascha Krüger, Maria Fernanda Sanchez-Goni and the other, anonymous, reviewer(s) for their contribution to the peer review of this work. Primary Handling Editors: Sze Ling Ho and Clare Davis.